Journal of Intelligent Material Systems and Structures
http://jim.sagepub.com

Effectiveness of Variable Stiffness Systems in Base-isolated Bridges Subjected to Near-fault Earthquakes: An Experimental and Analytical Study

Sanjay Sahasrabudhe and Satish Nagarajaiah

Journal of Intelligent Material Systems and Structures 2005; 16; 743
DOI: 10.1177/1045389X05054999

The online version of this article can be found at:
http://jim.sagepub.com/cgi/content/abstract/16/9/743

Published by:
SAGE Publications
http://www.sagepublications.com

Effectiveness of Variable Stiffness Systems in Base-isolated Bridges Subjected to Near-fault Earthquakes: An Experimental and Analytical Study

SANJAY SAHASRABUDHE[1] AND SATISH NAGARAJAIAH[2,*]

[1]*Structural Engineering Department, J. Ray McDermott Engineering, LLC, Houston, TX 77079, USA*

[2]*Departments of Civil and Environmental Engineering, and Mechanical Engineering and Materials Science Rice University, Houston, TX 77005, USA*

ABSTRACT: This article presents a novel semiactive independently variable stiffness (SAIVS) device, proposed for seismic response control of sliding base-isolated bridges. As a first step, force–displacement characteristics of the new SAIVS device are analytically and experimentally studied. It is demonstrated that the SAIVS device is capable of varying the stiffness, continuously and smoothly between minimum and maximum stiffnesses. This device is then incorporated into the sliding isolation system. In bridges, sliding isolation systems reduce pier drifts, but with increased bearing displacements. Such increased bearing displacements can be problematic under near-fault, large-velocity pulse-type earthquakes. To reduce bearing displacements, passive dampers are often incorporated into the isolation system. However, passive systems may result in increased pier drifts and isolation level forces. Semiactive variable stiffness systems, which can vary the period of the sliding isolated bridge in real-time, may reduce the bearing displacements and isolation level forces further than the passive systems; and hence, deserve investigation. In this study, the performance of a 1 : 20-scaled sliding base-isolated bridge model equipped with the new SAIVS device is analytically and experimentally studied under several near-fault earthquakes. A new control algorithm for the control of the SAIVS device is developed and implemented in shake table tests. It is shown that the semiactive SAIVS device reduces bearing displacements further than the passive cases, while maintaining isolation level forces at the same level as in the minimum stiffness case.

Key Words: base isolation, sliding isolation systems, variable stiffness, semiactive control, near-fault earthquakes.

INTRODUCTION

In buildings and bridges, sliding base-isolation systems provide an attractive option for reducing seismic response under near-fault earthquakes (Kelly, 1997). They, when used in bridges, reduce pier drifts and isolation level forces, but at the expense of increased isolation level displacements. Such increased bearing displacements can be problematic during near-fault, large-velocity pulse-type earthquakes (Nagarajaiah et al., 1993; Shen et al., 2004). Although base-isolated bridges are susceptible to near-fault earthquakes, their performance can be improved by incorporating supplemental passive fluid dampers into the isolation system, thus reducing bearing displacements. Providing such supplemental passive dampers can certainly reduce bearing displacements, but it may result in increased pier drifts and isolation level forces (Makris and Zhang, 2004). Semiactive variable stiffness systems can vary the period of the isolation system appropriately in real-time to reduce bearing displacements and forces further than the passive systems; and hence, deserve investigation. Base-isolation systems which utilize passive and/or semiactive controllable systems are commonly known as 'smart' or 'intelligent' base-isolation systems.

A number of different semiactive devices are proposed in the literature (Spencer and Nagarajaiah, 2003). Nagarajaiah (1994) studied applications of semiactive dampers in base isolated structures. Kawashima and Unjoh (1994) experimentally studied base-isolated bridges equipped with elastomeric bearings and controllable fluid dampers and showed their effectiveness in reducing the seismic response. Tsopelas et al. (1994) studied FPS sliding base-isolation systems equipped

*Author to whom correspondence should be addressed.
E-mail: nagaraja@rice.edu

1045-389X/05/09 0743–14 $10.00/0 DOI: 10.1177/1045389X05054999

with passive fluid dampers and showed their effectiveness. Yang et al. (1995) and Symans and Kelly (1999) have analytically investigated base-isolated bridges with elastomeric bearings and controllable fluid dampers, and showed their effectiveness in reducing seismic response. Jung et al. (2004) analytically studied the seismic performance of elastomerically base-isolated cable-stayed bridges equipped with semiactive magnetorheological (MR) fluid dampers (Carlson and Chrzan, 1994; Spencer et al., 1997), and showed their effectiveness. Agrawal et al. (2003) analytically studied applications of semiactive dampers in cable-stayed bridges and showed their effectiveness. Effectiveness of semiactive electrorheological (ER) dampers in elastomeric base-isolated structures has been studied by Makris (1997) and Gavin (2001), and shown to be effective in reducing seismic response. Sahasrabudhe and Nagarajaiah (2005a,b) studied effectiveness of magnetorheological (MR) dampers in sliding base isolated buildings and bridges and showed its effectiveness in reducing seismic response.

Kobori et al. (1993) have developed an active variable stiffness (AVS) system for seismic response control. In the AVS system, building stiffness is varied by engaging and disengaging the braces in each story of the structural framing system. The AVS system has been implemented in a full-scale structure in Tokyo, Japan. Nasu et al. (2001) have analytically investigated the performance of the AVS system. Their analytical study showed that by varying the stiffness intelligently, a nonresonant state can be achieved during an earthquake event, which results in reduced seismic response. One of the main limitations of the AVS system is the on–off switching of stiffness, which induces sudden changes in stiffness and corresponding changes in response. Resettable stiffness devices developed by Jabbari and Bobrow (2002) and Yang et al. (2000) are also of the on–off type. To overcome this limitation, a new semiactive, independently variable stiffness (SAIVS) device has been developed (Nagarajaiah and Mate, 1998). This device is capable of switching the stiffness continuously and smoothly. Nagarajaiah and Mate (1998) have shown the effectiveness of the small-scale SAIVS device in reducing both the displacement and the acceleration response, by switching the stiffness smoothly, due to nonresonant behavior. The objective of this study is to evaluate the effectiveness of variable stiffness systems in reducing seismic response of sliding base-isolated bridges under near-fault earthquakes. Moreover, there are no studies to date that evaluate variable stiffness systems in sliding base-isolated bridges. Narasimhan and Nagarajaiah (2005) analytically studied the effectiveness of the SAIVS device in reducing the seismic response of elastomeric base isolated buildings, and showed its effectiveness in reducing seismic response.

In this article, an analytical and experimental study of a 1 : 20-scaled base-isolated steel bridge model consisting of Teflon®–stainless steel sliding bearings and a medium-scale variable stiffness SAIVS device is presented. As a first step, force–displacement characteristics of the medium-scale SAIVS device are investigated analytically and experimentally. It is shown that the SAIVS device is capable of varying the stiffness continuously and smoothly between the minimum stiffness and maximum stiffness. The SAIVS device is then incorporated into the sliding base-isolation system. An analytical model of the bridge, with due consideration given to the nonlinearities of sliding bearings and SAIVS device, is developed. Using the analytical model developed, responses under a variety of near-fault earthquakes are computed. The analytical results are compared with the shake table test results (Sahasrabudhe, 2002). A new nonlinear control algorithm for the control of the SAIVS device and the bridge model is developed and implemented in shaking table tests. Responses of the passive cases are compared with that of the semiactive case. It is shown that the SAIVS device in semiactive controlled mode reduces isolation level displacements further than the passive maximum and minimum stiffness cases; while maintaining isolation level forces at the same level as in the case of the minimum stiffness case.

SEMIACTIVE INDEPENDENTLY VARIABLE STIFFNESS (SAIVS) DEVICE

The medium-scale SAIVS device is shown in Figure 1. The device consists of four sets of 15.24-cm-long springs and frictional elements arranged in a rhombus configuration as shown in Figure 1(a). Each of the four springs, connected to Joints 1–4, is located at an angle θ to the horizontal. An electromechanical actuator controlled with a computer is connected to Joint 1.

Joint 1 is fixed in the X-direction and can be placed at any desired position in the Y-direction by a linear electromechanical actuator and controller. Joint 2 is free to move in both the X- and Y-directions. Joints 3 and 4 are free to move in the X-direction only. The ends of the guide rail, on which Joint 2 moves, are attached to the shake table. The ends of the guide rail, on which Joints 3 and 4 move, are attached to the base. The electromechanical actuator is fixed to the base and can actuate in the Y-direction, thus moving Joint 1 to the required position.

The configuration of the SAIVS device can be switched to any desired position continuously and smoothly by positioning Joint 1, thus changing θ, using an attached electromechanical actuator. Each of the spring elements in the device is supported on the

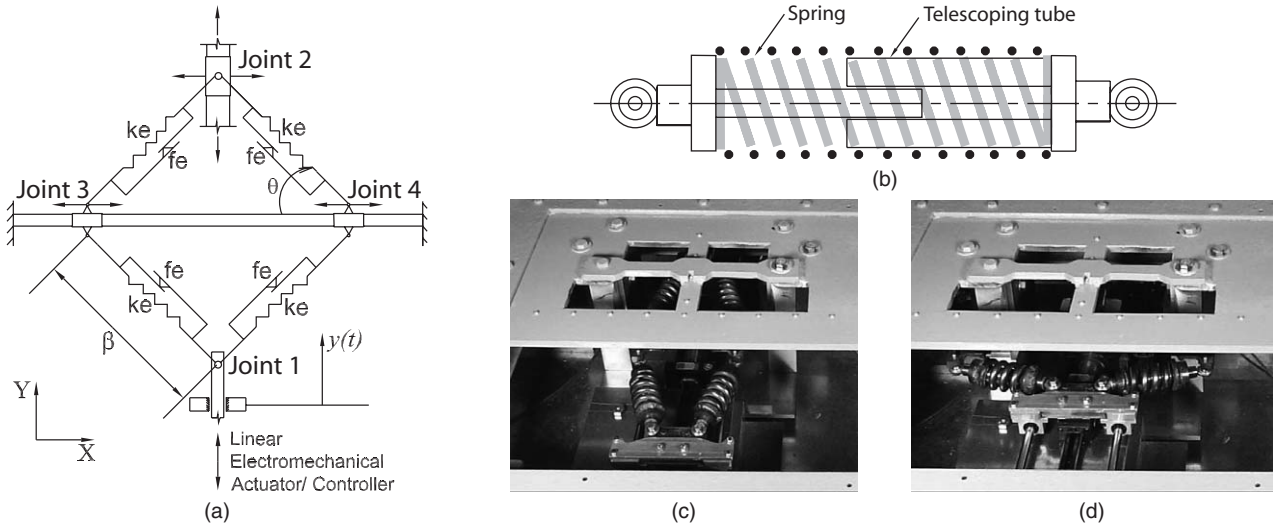

Figure 1. *Semiactive independently variable stiffness (SAIVS) device.*

inside by two telescoping tubes as shown in Figure 1(b). These tubes telescope into each other and allow extension and compression of the springs freely and prevent the springs from buckling. The telescoping tubes contribute to the frictional forces in the device, which is beneficial due to the resulting energy dissipation.

Based on its current position, the device generates the connection force at Joint 1 in the X-direction, due to the relative displacement between Joints 1 and 2. Figure 1(c) and (d) shows the device in the open and the closed positions, respectively. The device offers minimum resistance and has minimum stiffness in the open position (Figure 1(c)). The device offers maximum resistance and has maximum stiffness in the closed position (Figure 1(d)). The device can also be positioned in any configuration between the open and the closed positions; thus, the device is capable of varying the stiffness continuously and smoothly between the minimum and maximum stiffness states. The peak power required by the actuator is 104 W. The actuator requires voltage supply in the range of 0–4 V to change the configuration of the device from the open to the closed position.

Analytical Model for SAIVS Device

The analytical model is shown in Figure 1(a). It consists of four sets of springs and friction elements arranged in a rhombus configuration. Each of the four springs and the frictional elements in the device are located at an angle θ, to the horizontal. The device position in the Y-direction, $y(t)$, is used to compute the time-varying angle θ of the spring and friction elements. The device position $y(t)$ is monitored by a linear variable displacement transducer (LVDT) connected to Joint 1. The friction elements represent the friction in the telescoping tubes. The device develops forces due to the spring elements and the friction elements, at a given time, for a specific device position, which can be defined as:

$$F(t, u, \dot{u}) = F_{\mathrm{r}}(t) + F_{\mathrm{f}}(t, \dot{u}) \tag{1}$$

where, F_{r} is the restoring force due to spring deformation, F_{f} is the frictional force in the telescoping tubes, and $u(t)$ and $\dot{u}(t)$ are the relative displacement and relative velocity, respectively, between Joints 2 and 1 in the X-direction. The restoring force F_{r} at Joint 2 in the X-direction is given as:

$$F_{\mathrm{r}}(t) = k(t)u(t) = \{k_{\mathrm{e}} \cos^2 \theta(t)\}u(t) \tag{2}$$

where, $k_{\mathrm{e}} = 2984$ N/cm (1700 lb/in.) is the stiffness of a single spring and $\theta(t)$ is the time-varying angle of the spring elements with respect to horizontal for any given device position, given as:

$$\theta(t) = \sin^{-1}\left(\alpha - \frac{y(t)}{\beta}\right) \tag{3}$$

with $\alpha = 0.917$ being a nondimensional constant ($\alpha > y(t)/\beta$), β is the dimension of an individual spring element (15.24 cm) and $y(t)$ is the displacement ($\beta > y(t)$) of Joint 1 in the Y-direction. The frictional force at Joint 2 in the X-direction due to telescoping tubes, F_{f}, is given as:

$$F_{\mathrm{f}}(t, \dot{u}) = 2f_{\mathrm{e}} \cos\theta(t) \tag{4}$$

where,

$$f_{\mathrm{e}} = \frac{\alpha_{\mathrm{f}}}{2} z(\dot{u}') \tag{5}$$

Assuming that $\dot{u}'$, the velocity along the spring and friction elements, equal to $\dot{u}$, for small θ, and substituting Equation (5) in (4) we get:

$$F_{\mathrm{f}}(t, \dot{u}) = \alpha_{\mathrm{f}} z(\dot{u}) \cos\theta(t) \tag{6}$$

where, $\alpha_f = 66.88$ N (15 lb) and Wen's (1976) hysteresis variable z, used to model friction, is given by the differential equation:

$$\dot{z} = \frac{\left(\dot{u} - \gamma|\dot{u}|z|z| - \eta\,\dot{u}\,z^2\right)}{Y} \tag{7}$$

where, $\gamma = 0.9$, $\eta = 0.1$ are parameters of the hysteretic model with $\gamma + \eta = 1$ and $Y = 0.127$ cm is the 'yield' displacement.

Thus, in the open position, which corresponds to $y(t) = 0$, the device offers minimum stiffness of 373 N/cm. In the closed position, which corresponds to $y(t) = 10$ cm, the device offers maximum stiffness of 2510 N/cm. The springs can undergo a maximum deformation of 2.5 cm.

Experimental Test Setup of SAIVS Device

To study the force–displacement characteristics of the device, a setup, as shown in Figure 2, is designed. The SAIVS device is connected between the shake table and a fixed base. A load cell is connected to the fixed connecting rod (connected to a fixed frame) and the base. Hence the base remains fixed. The fixed base is supported by four Teflon®–stainless steel sliding bearings. The sliding bearings are supported by triaxial load cells, which independently measure friction forces in the bearings. The test setup is designed to apply a relative displacement between Joints 1 and 2 of the device. Joints 1, 3, and 4 are connected to carriages that slide on a system of rails. The rails are connected to a plate, which in turn is connected to the fixed base. A linear electromechanical actuator is connected to Joint 1 and the plate. A LVDT is also connected to Joint 1, which measures displacement $y(t)$ of the device. Joint 2 of the device is connected to another carriage and rail assembly, which is connected to the shaking table. A servohydraulic actuator displaces the shaking table based on a prescribed displacement time history of a given test. The SAIVS device acts as a connection between the moving shake table and the fixed base. The load cell, which is connected between the base and the connecting rod, measures the force generated by the SAIVS device and the total friction force in sliding bearings. The force generated by the SAIVS device is obtained by subtracting the friction force measured independently by four triaxial load cells from the force measured by the load cell that is connected between the base and the connecting rod. A LVDT is also connected between the shake table and the fixed frame to measure the relative displacement, $u(t)$, between Joints 1 and 2.

Analytical and Experimental Results

Using the setup shown in Figure 2, a series of tests were performed with harmonic ground excitation, with the SAIVS device position switching with sinusoidal, square, triangular, and random computer command signals. Figure 3 shows the sinusoidal relative displacement, of 1 Hz frequency, between Joints 2 and 1 (essentially the shake table displacement), SAIVS switching with a 0.1 Hz triangular electromechanical actuator command signal, and analytical and experimental SAIVS device force time histories. As evident from Figure 3(b), the SAIVS device is capable of tracking the commanded computer signal satisfactorily. From Figure 3(c) it is evident that the proposed analytical model captures the force generated by the device satisfactorily. Figure 4 shows the experimental and analytical force displacement loops of the SAIVS device switching with triangular command signal. From the figure it is evident that the SAIVS device is capable of varying the stiffness, continuously and smoothly, between the open (minimum stiffness state) and the closed (maximum stiffness state) positions. This unique feature of the device is not available with the conventional on–off type variable stiffness systems, such as the AVS system (Kobori et al., 1993). It is also evident from the figure that the device is capable of generating time-varying and nonlinear-restoring forces. Figure 5 shows the time histories of the relative displacement of 0.5 Hz frequency, the SAIVS device switching with a 0.5 Hz square command signal, and the analytical and

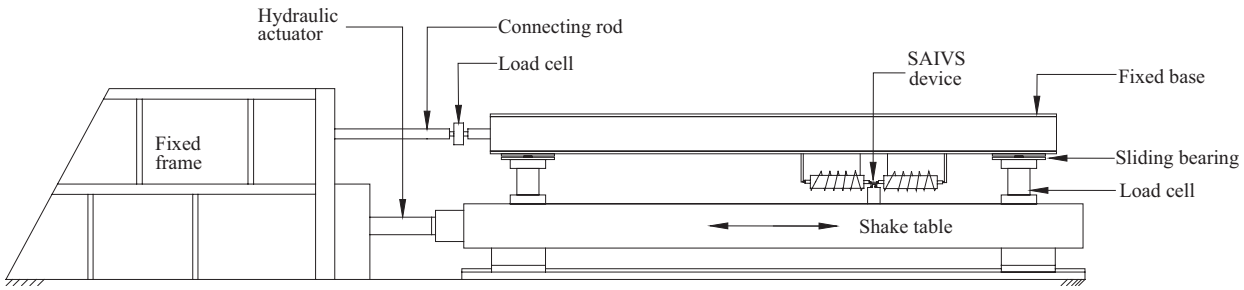

Figure 2. *SAIVS device calibration setup.*

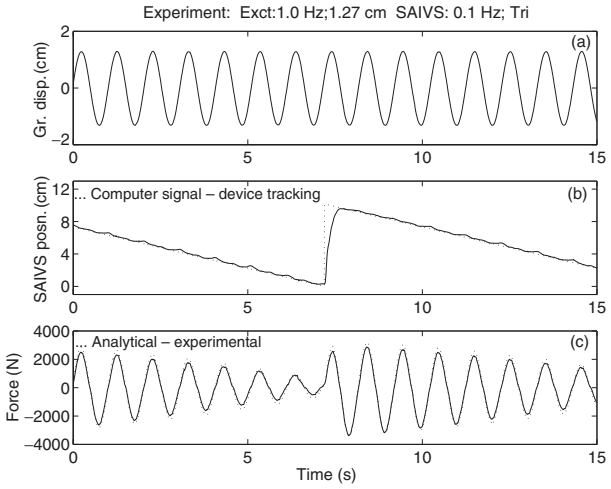

Figure 3. *Time histories of (a) relative displacement; (b) command signal to the SAIVS device and SAIVS position; and (c) analytical and experimental force in the SAIVS device.*

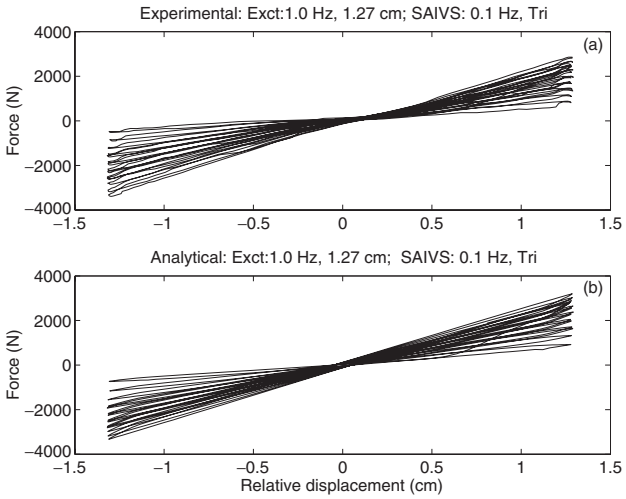

Figure 4. *Experimental and analytical force–displacement response of SAIVS device to harmonic excitation of 1.0 Hz: SAIVS switching with a triangular signal of 0.1 Hz.*

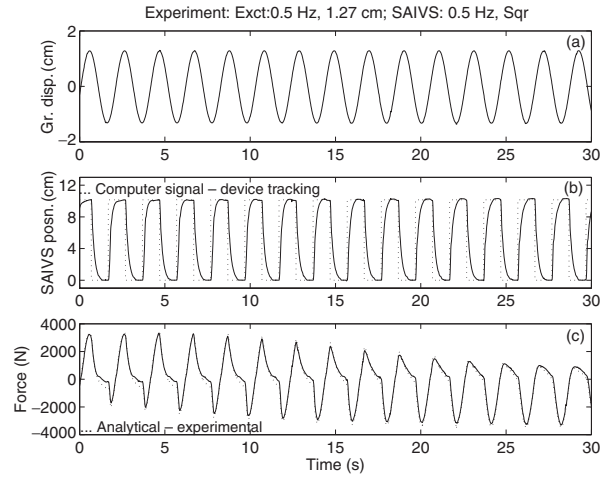

Figure 5. *Time histories of (a) relative displacement; (b) command signal to the SAIVS device and SAIVS position; and (c) analytical and experimental forces in the SAIVS device.*

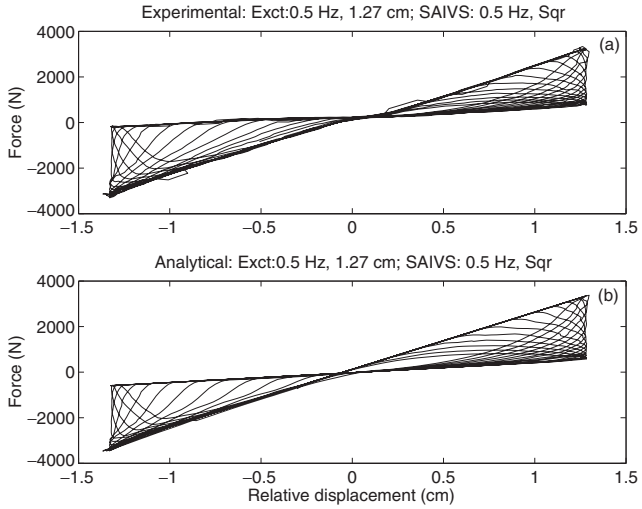

Figure 6. *Experimental and analytical force–displacement response of SAIVS device to a harmonic excitation of 0.5 Hz: SAIVS switching with a square signal of 0.5 Hz.*

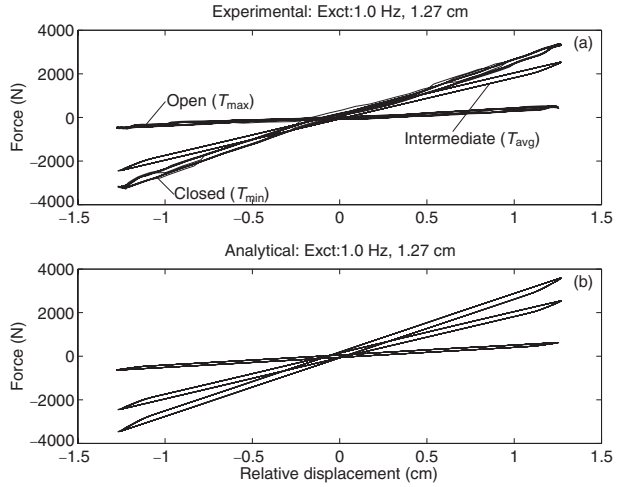

Figure 7. *Experimental and analytical force–displacement response of SAIVS device in passive open (T_{max}), passive closed (T_{min}), and passive intermediate (T_{avg}) positions.*

experimental SAIVS force time histories. It is to be noted from Figures 3(b) and 5(b) that the SAIVS device is capable of switching with a variety of commanded signals effectively. Figure 6 shows the experimental and analytical force–displacement behavior of the SAIVS device switching with a square command signal. The rich and intricate force–displacement characteristics of the device are notable.

Figure 7 shows the force–displacement behavior of the device under sinusoidal relative displacement of frequency 1 Hz; with the device in the passive open ($T_{\max}$), passive closed ($T_{\min}$), and passive intermediate (T_{avg}) positions. As evident from the figure, the device offers a minimum stiffness of 373 N/cm in the passive open position; whereas, it offers a maximum stiffness of 2510 N/cm in the passive closed position.

1:20 SCALE BRIDGE MODEL WITH SLIDING BEARINGS AND SAIVS DEVICE

Based on the laws of artificial mass simulation (Mills et al., 1979) shown in Table 1, a single span 1:20-scaled bridge model has been designed and fabricated (Sahasrabudhe, 2002). The bridge model, shown in Figures 8 and 9 has a clear span of 1.83 m, width 0.89 m, and height 0.96 m. Weight of the deck is 12.48 kN and each of the piers weigh 0.53 kN. At model scale, the bridge is designed to have a natural period of 0.1 s in the nonisolated case i.e., 0.45 s at prototype scale. The bridge model has four sliding bearings, consisting of Teflon®–stainless steel interface (Figure 8(a)). The sliding bearings decouple the deck from the piers. The sliding bearings are supported by four triaxial load cells which are mounted on the top of the piers. The triaxial load cells measure frictional forces transmitted from the deck to the piers (Figure 9(a)). The sliding bearings have a dynamic coefficient of friction of 6% at low velocities and 13% at high velocities (Sahasrabudhe and Nagarajaiah, 2005b). The SAIVS device is connected between the deck and the right pier as shown in Figure 9(b). In the isolated case, the bridge model has a period of 1.2 s with the SAIVS device in fixed open position and 0.46 s with the SAIVS device in fixed closed position. A passive damper is also connected between the deck and the left pier (Figure 8(a)). The bridge model was instrumented with LVDTs and accelerometers at both the piers and the deck to measure displacement and acceleration response (Figure 8(a)). A dSPACE system with MATLAB/Simulink was used to perform data acquisition and control. The schematics of experimental data acquisition and control system are shown in Figure 8(a). Figure 8(b) shows the block diagram of the proposed control strategy.

Table 1. Scaling factors.

Parameter	Scaling factors	1:20 model
Length	l_r	1/20
Time	$\sqrt{l_r}$	$1/\sqrt{20}$
Displacement	l_r	1/20
Velocity	$\sqrt{l_r}$	$1/\sqrt{20}$
Acceleration	1	1
Force	l_r^2	1/400

ANALYTICAL AND EXPERIMENTAL PROGRAM

To evaluate the effectiveness of the SAIVS device, an analytical and experimental study was carefully planned.

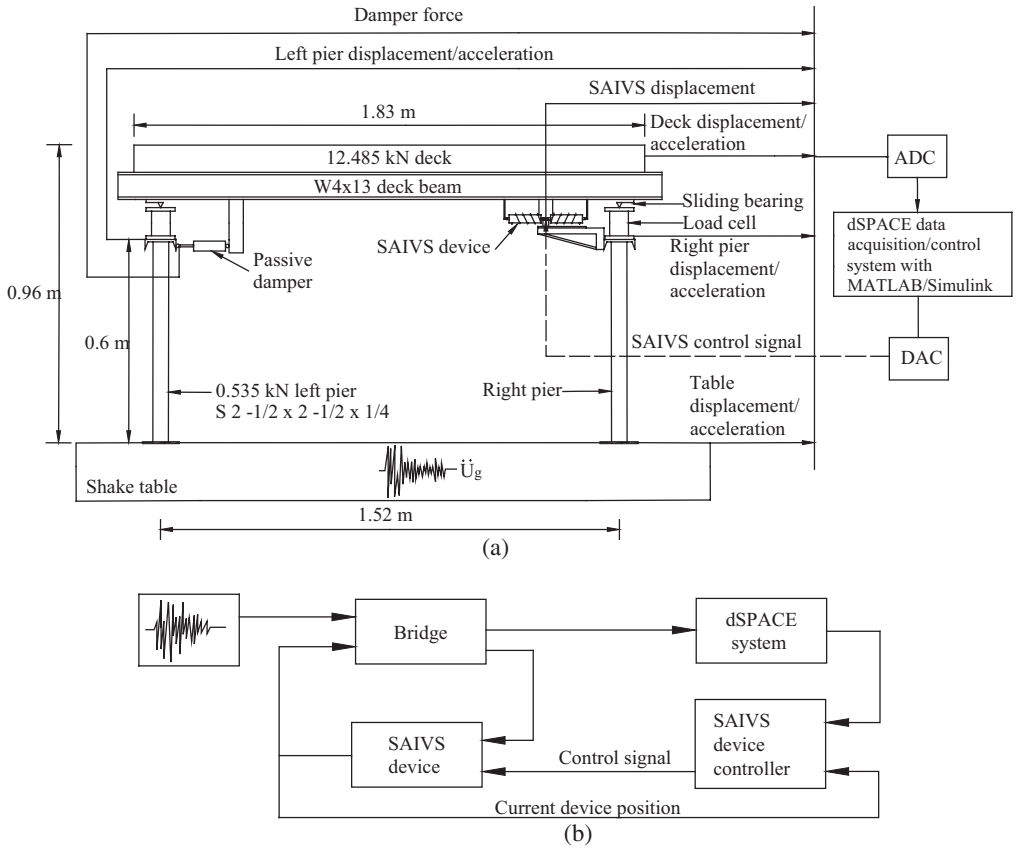

Figure 8. *(a) Sliding isolated bridge model scaled 1:20 with SAIVS device and block diagram of data acquisition and control system and (b) block diagram of control strategy.*

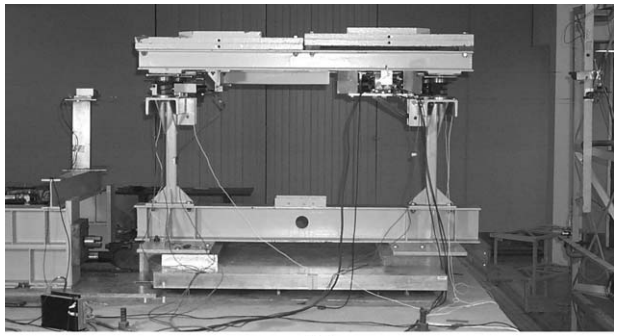

(a)

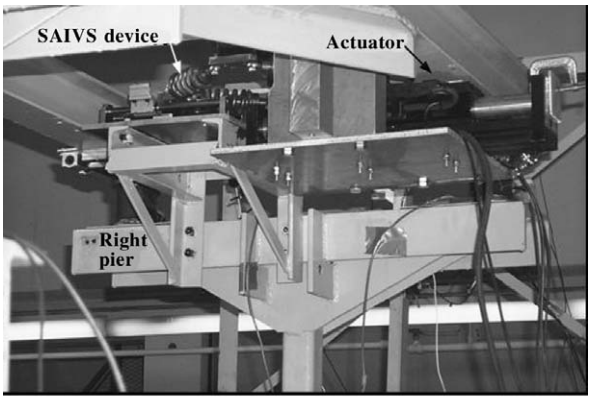

(b)

Figure 9. *(a) Sliding isolated bridge model scaled 1 : 20 with the SAIVS device and (b) close-up view of the SAIVS device connected between deck and right pier.*

Shake table tests were performed under isolated case with: (1) SAIVS device in fixed open position – passive minimum stiffness condition, (2) SAIVS device in fixed closed position – passive maximum stiffness condition, and (3) semiactive controlled case in which the SAIVS device position is switched based on the control algorithm developed. Shake table tests were performed with the following scaled earthquakes:

1. El Centro S00E Earthquake (May 18, 1940), peak acceleration: 0.645 g.
2. Northridge Newhall Earthquake, Channel 1 90° (Jan. 17, 1994), peak acceleration: 0.75 g.
3. Northridge Sylmar Earthquake, Channel 1 90° (Jan. 17, 1994), peak acceleration: 0.99 g.

The El Centro earthquake exhibits characteristics of far-field motions although it was recorded near-fault. As per Table 1, the earthquake signals were compressed by a timescale factor of $1/\sqrt{20}$. The peak accelerations were scaled from original recorded values.

ANALYTICAL MODEL OF THE SLIDING ISOLATED BRIDGE MODEL

An analytical model of the bridge, with due consideration given to the nonlinearities of frictional sliding bearings, SAIVS device, and the passive damper, is developed (Sahasrabudhe, 2002). The mass of the deck is 12.72 N s^2/cm. The mass of each pier is 0.54 N s^2/cm. The equations of motion are:

$$m_{\mathrm{d}}\ddot{U}_{\mathrm{d}} + F_{\mathrm{b1}} + F_{\mathrm{b2}} + F_{\mathrm{SAIVS}} + F_{\mathrm{Damper}} = -m_{\mathrm{d}}\ddot{U}_{\mathrm{g}} \quad (8)$$

$$m_{\mathrm{p1}}\ddot{U}_{\mathrm{p1}} + F_{\mathrm{p1}} - F_{\mathrm{b1}} - F_{\mathrm{Damper}} = -m_{\mathrm{p1}}\ddot{U}_{\mathrm{g}} \quad (9)$$

$$m_{\mathrm{p2}}\ddot{U}_{\mathrm{p2}} + F_{\mathrm{p2}} - F_{\mathrm{b2}} - F_{\mathrm{SAIVS}} = -m_{\mathrm{p2}}\ddot{U}_{\mathrm{g}} \quad (10)$$

where, U_{d}, U_{p1},U_{p2} are the deck, left pier, and right pier displacements relative to shake table, respectively. $\ddot{U}_{\mathrm{g}}$ is ground acceleration. $\ddot{U}_{\mathrm{d}}$,$\ddot{U}_{\mathrm{p1}}$,$\ddot{U}_{\mathrm{p2}}$ are deck, left pier, and right pier accelerations, respectively. The relative displacement between the deck and pier i, $U_{\mathrm{b}i}$, is obtained as: $U_{\mathrm{b}i} = U_{\mathrm{d}} - U_{\mathrm{p}i}$. m_{d}, m_{p1}, m_{p2} are deck, left pier, and right pier masses, respectively. $F_{\mathrm{SAIVS}} = f_{\mathrm{SD}}$ is the force generated by the SAIVS device, which is obtained by Equation (1), by replacing u with U_{b2} which is the relative deck–right pier displacement. F_{b1} and F_{b2} are the frictional forces in the sliding bearings at left and right piers, respectively, with $f_{\mathrm{s}} = F_{\mathrm{b1}} + F_{\mathrm{b2}}$. The frictional forces in sliding bearings are given as: $F_{\mathrm{b}i} = \mu_i w_i z_i$, where μ_i is the coefficient of dynamic sliding friction at pier i given by Equation (11) (Nagarajaiah et al., 1991a), w_i is the normal load on the sliding bearing at pier i.

$$\mu_i = f_{\mathrm{max\_}i} - (f_{\mathrm{max\_}i} - f_{\mathrm{min\_}i})e^{-(a_i \mathrm{abs}(\dot{U}_{\mathrm{b}i}))} \quad (11)$$

where, $f_{\mathrm{max\_}i} = 0.13$, $f_{\mathrm{min\_}i} = 0.06$, and $a_i = 0.2362$ s/cm.

The hysteresis variable z (Wen, 1976) for friction is obtained by solving Equation (12) with $Y_i = 0.127$ cm – the small yield displacement of Teflon® bearing before sliding, $\gamma = 0.9$ and $\eta = 0.1$.

$$Y_i\dot{z}_i + \gamma|\dot{U}_{\mathrm{b}i}|z_i|z_i| + \eta\dot{U}_{\mathrm{b}i}z_i^2 - \dot{U}_{\mathrm{b}i} = 0 \quad (12)$$

F_{Damper} is the nonlinear force generated in the passive damper, which is given as:

$$f_{\mathrm{c}} = F_{\mathrm{Damper}} = f_{\mathrm{D}}z + C\dot{U}_{\mathrm{b1}} + kU_{\mathrm{b1}} \quad (13)$$

where, $f_{\mathrm{D}} = 893.3$ N, $C = 18.94$ N s/cm, and $k = 8.24$ N/cm. The hysteresis variable z for the passive damper is obtained by solving Equation (12) with $Y_i = 0.165$ cm. In Equation (13), U_{b1} is the deck–left pier relative displacement. F_{p1}, F_{p2} are resisting forces in the piers which are given as: $F_{\mathrm{p}i} = k_{\mathrm{p}i}U_{\mathrm{p}i} + c_{\mathrm{p}i}\dot{U}_{\mathrm{p}i}$, where $k_{\mathrm{p}i}$ and $c_{\mathrm{p}i}$ are stiffness and damping coefficient of pier i. The piers are assumed as lumped mass systems.

The corresponding state equation, measured output equation, and regulated output equation are as follows:

$$\dot{\boldsymbol{x}}(t) = \boldsymbol{A}\boldsymbol{x}(t) + \boldsymbol{B}f_{\mathrm{c}}(t) + \boldsymbol{B}f_{\mathrm{s}}(t) + \boldsymbol{B}f_{\mathrm{SD}}(t) + \boldsymbol{E}\ddot{U}_{\mathrm{g}}(t) \quad (14)$$

$$\boldsymbol{y}(t) = \boldsymbol{C}_{\mathrm{m}}\boldsymbol{x}(t) + \boldsymbol{D}_{\mathrm{m}}f_{\mathrm{c}}(t) + \boldsymbol{D}_{\mathrm{m}}f_{\mathrm{s}}(t) + \boldsymbol{D}_{\mathrm{m}}f_{\mathrm{SD}}(t) + \boldsymbol{E}_{\mathrm{m}}\ddot{U}_{g}(t) \quad (15)$$

$$\boldsymbol{z}(t) = \boldsymbol{C}_{\mathrm{z}}\boldsymbol{x}(t) + \boldsymbol{D}_{\mathrm{z}}f_{\mathrm{c}}(t) + \boldsymbol{D}_{\mathrm{z}}f_{\mathrm{s}}(t) + \boldsymbol{D}_{\mathrm{z}}f_{\mathrm{SD}}(t) + \boldsymbol{E}_{\mathrm{z}}\ddot{U}_{\mathrm{g}}(t) \quad (16)$$

where, $\boldsymbol{A}$, $\boldsymbol{B}$, $\boldsymbol{C}_{\mathrm{m}}$, $\boldsymbol{C}_{\mathrm{z}}$, $\boldsymbol{D}_{\mathrm{m}}$, $\boldsymbol{D}_{\mathrm{z}}$, $\boldsymbol{E}$, $\boldsymbol{E}_{\mathrm{m}}$, $\boldsymbol{E}_{\mathrm{z}}$, $\dot{\boldsymbol{x}}(t)$, $\boldsymbol{x}(t)$, $\boldsymbol{y}(t)$, $\boldsymbol{z}(t)$ are appropriately defined system matrices or vectors.

The nonlinear equations of motion are solved using an iterative pseudo-force method (Nagarajaiah et al., 1991a, b). The equations of motion (Equations (8)–(10)) are solved using the unconditionally stable Newmark's constant-average-acceleration method. The differential equations governing the behavior of the nonlinear sliding isolation elements, passive damper, and the SAIVS device are solved using the unconditionally stable semi-implicit Runge–Kutta method. An iterative procedure consisting of corrective pseudo forces is employed within each time step until equilibrium is achieved.

CONTROL ALGORITHM FOR SAIVS DEVICE

A newly developed nonlinear control algorithm is presented next. Based on Equation (1), which governs the mechanical behavior of SAIVS device:

$$K_{\mathrm{SAIVS}} = k_{\mathrm{e}}\cos^2\theta(t) \quad (17)$$

Introducing a time shift, τ, we get:

$$K_{\mathrm{SAIVS}} = k_{\mathrm{e}}\cos^2\theta(t-\tau) \quad (18)$$

where $K_{\min} < K_{\mathrm{SAIVS}} < K_{\max}$, and

$$\theta(t-\tau) = \sin^{-1}\left(\alpha - \frac{y(t-\tau)}{\beta}\right) \quad (19)$$

with $\alpha = 0.917$ being a nondimensional constant ($\alpha > y(t-\tau)/\beta$)), β is the dimension of an individual spring element (15.24 cm) and $y(t-\tau)$ is the displacement ($\beta > y(t-\tau)$) of Joint 1, connected to the linear electromechanical actuator. The displacement $y(t-\tau)$ required to control the SAIVS device is given by:

$$y(t-\tau) = \sum_{i=j}^{k} \frac{\gamma}{(k-j)} \left| U_{\mathrm{b2}}(t-\tau_i) \right|^{\lambda} \quad (20)$$

where $\lambda = 0.6$ is a nondimensional constant ($\lambda < 1$) and γ is a constant with appropriate dimension so that $y(t-\tau)$ is in inches, t is the current time, $\tau_i = iT_{\mathrm{avg}}/100$, and $\tau = jT_{\mathrm{avg}}/100$, where T_{avg} is the average period given by Equation (21), $j = 8$ and $k = 18$, and U_{b2} is the deck–right pier relative displacement.

$$T_{\mathrm{avg}} = 2\pi\sqrt{\frac{m_{\mathrm{total}}}{(k_{\min} + k_{\max})/2}} \quad (21)$$

where $k_{\max}$ = maximum stiffness of the SAIVS device (2510 N/cm), $k_{\min}$ = minimum stiffness of the SAIVS device (373 N/cm), and m_{total} = total mass of the system. Also, $t \geq 0$ and $t > \tau$ in Equations (19) and (20). For $t \leq \tau$

$$K_{\mathrm{SAIVS}} = k_{\mathrm{e}} \quad (22)$$

The relative displacement U_{b2}, needed in Equation (20), can be readily measured by connecting a LVDT between the deck and the right pier.

The control algorithm (Equation (20)) is designed such that the angle $\theta(t)$ is a nonlinear function of the moving average of relative deck–right pier displacement. The control objective is to make spring force a nonlinear function of the relative deck–right pier displacement. The nonlinear function is designed to simulate softening tangential stiffness at larger relative displacements, with eventual negative tangential stiffness at peak relative displacements to reduce the response. A moving average of the relative displacement was chosen to ensure smooth stiffness variation and to reduce the effects of measurement noise. The exponent, $\lambda = 0.6$, was chosen to simulate softening tangential stiffness and was arrived at by performing a series of analytical simulations for the chosen earthquakes, which resulted in the least response. The coefficient $\gamma = 3.5$ was chosen to ensure that the SAIVS position is within 10 cm. The SAIVS position is bounded by $\approx$1 cm in the open position and 10 cm in the closed position.

EXPERIMENTAL AND ANALYTICAL RESULTS

The results are presented in Table 2 in the form of peak values of relative displacement responses, peak total force at the isolation level (total of friction, SAIVS device, and passive damper force normalized by deck weight), and deck acceleration. The results under (1) Sylmar 90, (2) Newhall 90, and (3) El Centro earthquakes are discussed in detail. The peak values of experimental relative deck–right pier displacement response, as a function of peak table acceleration, with SAIVS passive open – minimum stiffness – case, SAIVS passive closed – maximum stiffness – case, and semiactive control cases are presented in Figure 10. Figure 11 shows the total force at the isolation level

Table 2. Comparison of experimental and analytical response of the sliding isolated bridge model with SAIVS device (values in parentheses indicate the percentage reductions in passive closed and controlled cases compared to passive open case).

Earthquake	SAIVS device	Deck–left pier (cm)		Deck–right pier (cm)		Deck–table (cm)		Left pier–table (cm)		Right pier–table (cm)		Total force at isolation level/weight		Deck acceleration (g)	
		Expt.	Anly.	Expt.	Anly.	Expt.	Anly.	Expt.	Anly.	Expt.	Anly.	Expt.	Anly.	Expt.	Anly.
El Centro	Open	1.294	1.323	1.26	1.295	1.384	1.452	0.18	0.26	0.16	0.21	0.271	0.27	0.318	0.3
El Centro	Closed	1.03	1.05	0.92	0.9	1.113	1.16	0.212	0.296	0.226	0.272	0.35	0.345	0.38	0.38
		(−20%)	(−21%)	(−27%)	(−30%)	(−20%)	(−20%)	(18%)	(14%)	(41%)	(30%)	(29%)	(28%)	(19%)	(27%)
El Centro	Control	1.00	1.00	0.91	0.98	1.07	1.15	0.18	0.275	0.19	0.22	0.277	0.26	0.355	0.31
		(−23%)	(−24%)	(−28%)	(−24%)	(−23%)	(−21%)	(0%)	(6%)	(19%)	(5%)	(2%)	(4%)	(12%)	(3%)
Sylmar 90	Open	1.641	1.642	1.604	1.602	1.76	1.79	0.21	0.269	0.19	0.213	0.284	0.29	0.36	0.327
Sylmar 90	Closed	1.703	1.57	1.44	1.35	1.792	1.722	0.21	0.28	0.38	0.42	0.461	0.433	0.494	0.474
		(4%)	(−4%)	(−10%)	(−16%)	(2%)	(−4%)	(0%)	(4%)	(100%)	(97%)	(62%)	(49%)	(37%)	(45%)
Sylmar 90	Control	1.361	1.375	1.218	1.31	1.44	1.558	0.193	0.315	0.241	0.26	0.331	0.331	0.446	0.406
		(−17%)	(−16%)	(−24%)	(−18%)	(−18%)	(−13%)	(−8%)	(17%)	(27%)	(22%)	(17%)	(14%)	(24%)	(24%)
Newhall 90	Open	1.135	1.03	1.111	1.1	1.196	1.134	0.183	0.29	0.135	0.201	0.29	0.3	0.304	0.34
Newhall 90	Closed	1.438	1.313	1.222	1.164	1.498	1.406	0.2	0.29	0.293	0.35	0.414	0.445	0.373	0.457
		(27%)	(27%)	(10%)	(6%)	(25%)	(24%)	(9%)	(0%)	(117%)	(74%)	(43%)	(48%)	(23%)	(34%)
Newhall 90	Control	1.09	1.08	1.03	1.00	1.148	1.204	0.223	0.301	0.155	0.245	0.29	0.3	0.286	0.378
		(−4%)	(5%)	(−7%)	(−9%)	(−4%)	(6%)	(22%)	(4%)	(15%)	(22%)	(0%)	(0%)	(−6%)	(11%)

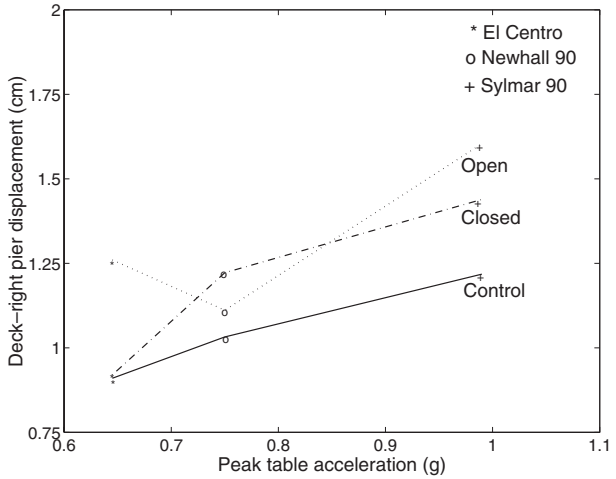

Figure 10. *Comparison of experimental peak relative deck–right pier displacement response under various earthquakes.*

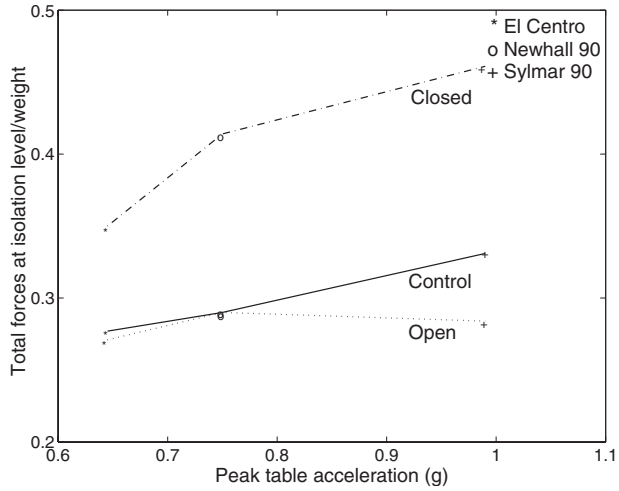

Figure 11. *Comparison of experimental total force at isolation level/ weight under various earthquakes.*

normalized by deck weight, as a function of peak table acceleration, under passive open, passive closed, and semiactive controlled cases.

As evident from Table 2 and Figures 10 and 11, in the case of Sylmar 90 earthquake, the deck–right pier displacement in the passive closed (maximum stiffness) case is reduced by 10% when compared with the passive open (minimum stiffness) case. However, the passive closed case results in 62% increase in the total force at the isolation level, when compared to the passive open case. As expected, increased stiffness in the passive closed case attracts more forces. The semiactive controlled case, shown in Figures 10 and 11, further reduces the deck–right pier displacement by 15% when compared to the passive closed case, yet maintaining the total force at the isolation level significantly less than the passive closed case (refer Table 2). Thus the semiactive control case, with intelligent variation of stiffness, reduces the relative deck–right pier displacement response further than the passive open and closed cases, while maintaining the isolation level forces at the same level as the passive open case. Such reductions in displacements and forces reveal the effectiveness of the SAIVS device. A similar set of observations can be obtained from the analytical results presented in Table 2.

Table 2 also shows the peak values of relative right pier–shake table displacement, and deck acceleration. Note that the passive closed case, as a result of increased forces, results in significantly increased right pier displacements, thus undermining the beneficial effects of sliding isolation system (refer Table 2). The semiactive control case maintains the right pier displacement at the same level as the passive open case. The control case also maintains the deck acceleration within bounds of the passive open and closed cases.

The experimental results under Newhall 90 and El Centro earthquakes are also presented in Table 2 and Figures 10 and 11. The semiactive controlled case results in the least relative deck–right pier displacement response, when compared with the passive open and passive closed cases, in both earthquakes. In Newhall 90, the control case reduces the deck–right pier displacement by 7% when compared to the passive open case and by 16% when compared to the passive closed case. In case of El Centro earthquake, the control case gives a total 28% reduction in relative deck–right pier displacement. Thus in Newhall 90 and El Centro, the controlled case results in the least relative deck–right pier displacement response, yet maintaining total force at the isolation level at the same level as in the passive open case (see Table 2 and Figure 11). It is noteworthy that the maximum deck–right pier displacement response in Sylmar 90 and El Centro occur in the passive open case, whereas it occurs in the passive closed case in Newhall 90. The variable stiffness case, however, uniformly reduces the displacements and forces in all three earthquakes. Thus, the newly developed control algorithm is effective in reducing the displacements and total forces. This demonstrates the salient features and potential of the SAIVS system.

The shaking table test results are presented in Figures 12–19 in the form of relative displacement time history responses, total force at the isolation level as a function of relative deck–right pier displacement responses, SAIVS device force as a function of relative deck–right pier displacement responses, SAIVS device position and deck acceleration time history responses for Sylmar 90 and Newhall 90 excitations. Corresponding analytical results are also presented in Figures 13–15, and 17–19. Note that to highlight the differences clearly, a 0.06 s time shift is introduced in the passive open and closed case relative displacement time histories shown in Figures 12 and 16. A comparison of the experimental relative displacement time histories for

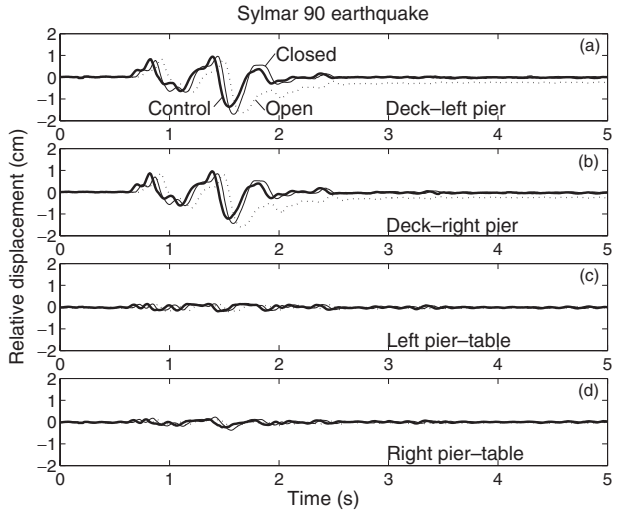

Figure 12. *Experimental relative displacement time history responses under Sylmar 90 earthquake.*

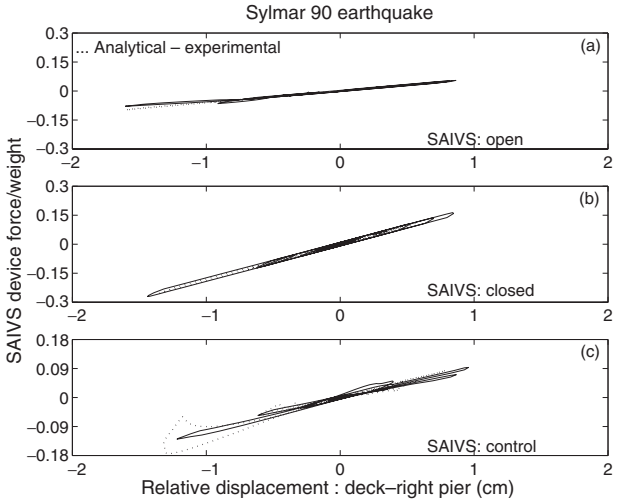

Figure 14. *Comparison of experimental and analytical SAIVS force/weight as a function of the relative deck–right pier displacement under Sylmar 90 earthquake.*

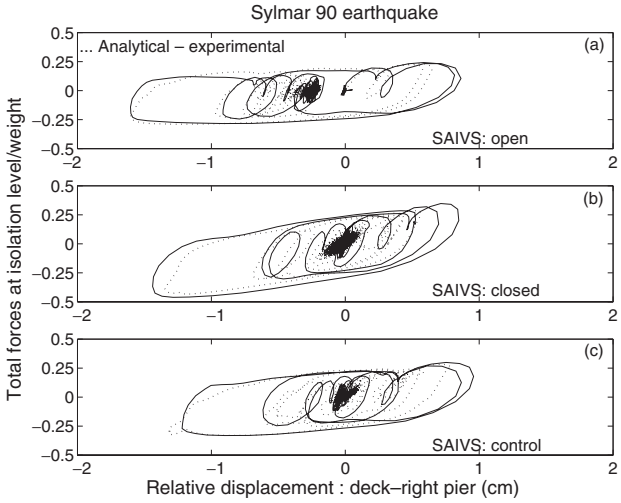

Figure 13. *Comparison of experimental and analytical total force at isolation level/weight as a function of relative deck–right pier displacement under Sylmar 90 earthquake.*

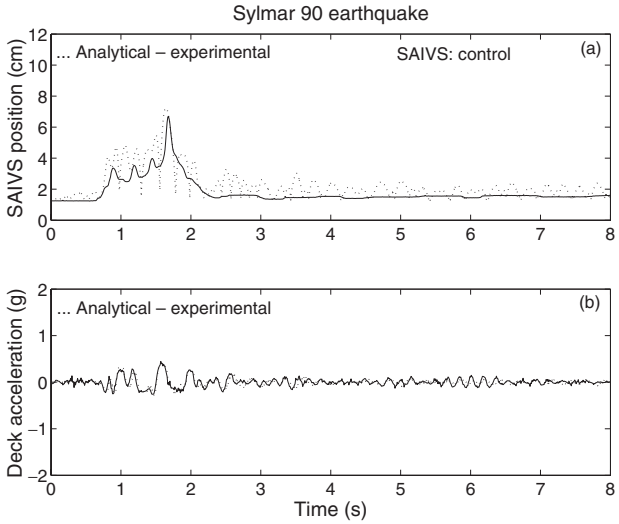

Figure 15. *Comparison of experimental and analytical SAIVS switching and deck acceleration time histories under Sylmar 90 earthquake.*

Sylmar 90 earthquake, presented in Figure 12, indicates dominant deck–pier displacements and significantly smaller pier displacements – a typical first mode response. It is evident from Figure 12 that the controlled case results in reductions in the relative deck–right pier displacements. Figure 13 presents a comparison of the analytical and experimental total forces at the isolation level as a function of the relative deck–right pier displacement responses under Sylmar 90 earthquake, with passive open, passive closed, and semiactive variable stiffness cases. It is evident from Figure 13(c) that the controlled case results in reductions in relative deck–right pier displacements and total forces. Corresponding analytical results presented in Figure 13 reveal that the analytical model captures the response of the bridge model satisfactorily. Figure 14 presents the SAIVS device force as a function of the relative deck–right pier displacement loops under Sylmar 90 earthquake, with passive open, passive closed, and semiactive control cases. It is evident from Figure 14(c) that the SAIVS device in the controlled mode varies the stiffness continuously and smoothly as commanded by the control algorithm and reduces the response. The softening tangential stiffness is evident in both experimental and analytical force–displacement loops in Figure 14(c); however, the eventual negative tangential stiffness is evident only in the analytical force–displacement loops at peak relative displacements. The softening tangential stiffness (Figure 14(c)) is the primary reason for the reduction of response, essentially preventing excessive strain energy from being stored in the SAIVS device at larger relative displacements, coupled with energy

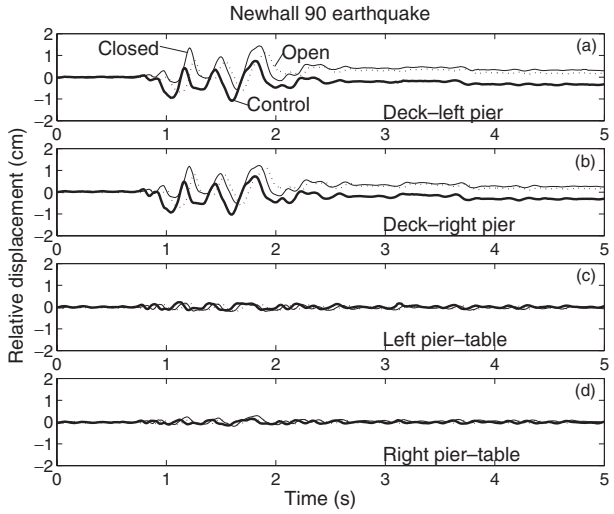

Figure 16. *Experimental relative displacement time history responses under Newhall 90 earthquake.*

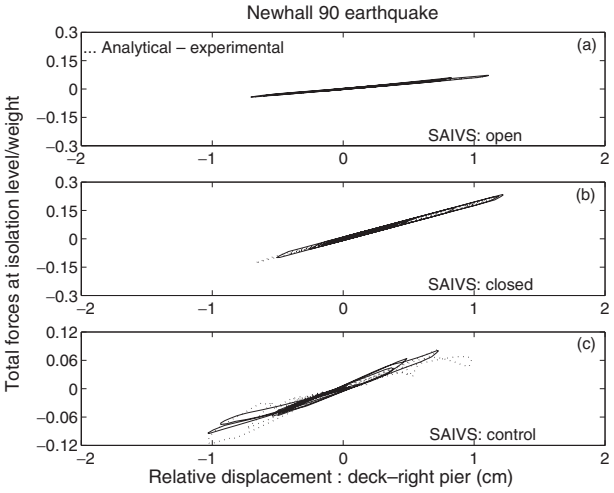

Figure 18. *Comparison of experimental and analytical SAIVS force as a function of relative deck–right pier displacement under Newhall 90 earthquake.*

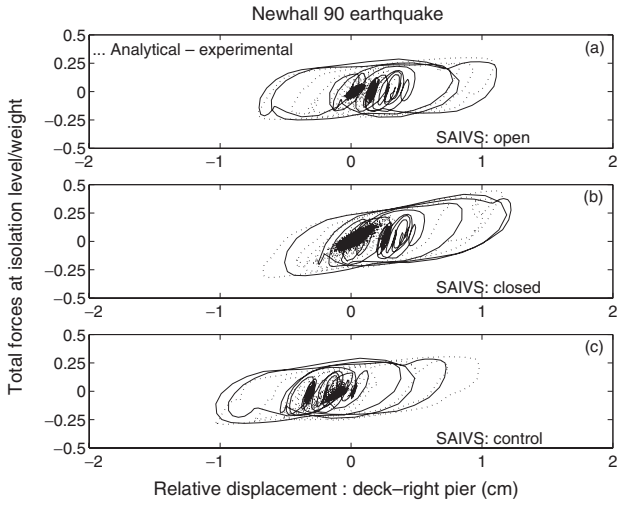

Figure 17. *Comparison of experimental and analytical total force at isolation level/weight as a function of relative deck–right pier displacement under Newhall 90 earthquake.*

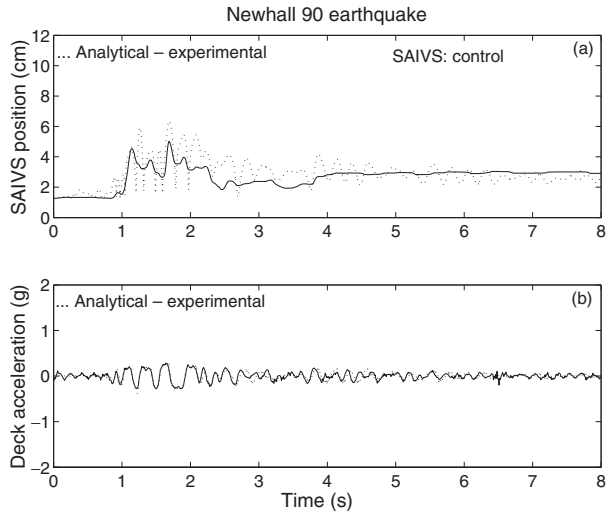

Figure 19. *Comparison of experimental and analytical SAIVS switching and deck acceleration time histories under Newhall 90 earthquake.*

dissipation resulting in an effective system. This is further evident in Figures 12(b) and 15(a), wherein the stiffness of the device is smaller when the peak relative deck–right pier displacement occurs at 1.5 s, following which the stiffness increases at 1.7 s when the relative displacement is smaller. Figure 15 presents SAIVS switching and deck acceleration time history responses, in the controlled case, under Sylmar 90 earthquake. The deck acceleration time histories presented in Figure 15(b) reveal that no abrupt acceleration spikes occur as the SAIVS device varies stiffness continuously and smoothly.

From Figures 16–19, a similar set of observations, as in the Sylmar 90 case, can be obtained from the responses under Newhall 90 earthquake. Again, the softening tangential stiffness – followed by negative tangential stiffness at peak relative displacement in the analytical force displacement loops (Figure 18(c)) – is the primary reason for reduction in response. It is evident from Table 2 that the pier displacements and deck accelerations are substantially higher in the SAIVS closed case. However, the semiactive controlled case maintains the pier displacements and deck acceleration either less than or within bounds of peak values of passive open and passive closed cases. From peak values of responses presented in Table 2, and Figures 13–15 and 17–19, it is evident that the proposed analytical model captures the response of the bridge model satisfactorily.

It can be concluded that the SAIVS device in the semiactive controlled case reduces the deck–right pier displacements further than the passive open and passive

closed cases, yet maintaining the isolation level forces at the same level as the passive open case. The ability of the SAIVS device to vary the stiffness continuously and smoothly results in reductions in displacements and forces. The proposed control algorithm reduces the response in the fault-parallel components of the earthquakes considered in this study.

CONCLUSIONS

The efficacy of a novel semiactive independently variable stiffness (SAIVS) device, in reducing seismic response of a smart sliding base-isolated bridge model, is analytically and experimentally studied and shown to be effective. The analytical and experimental force–displacement behavior of the SAIVS device reveals that the device is capable of varying stiffness continuously and smoothly. This unique feature of the device is not available with the conventional on–off type variable stiffness systems. It is evident from the analytical and experimental study that the SAIVS device with a suitable control algorithm, when incorporated into the sliding base-isolation system, reduces bearing displacements further than the passive open and passive closed cases, while significantly reducing isolation level forces when compared to the passive closed case. The main conclusions of this study are: (1) in sliding base-isolated bridges, increasing the stiffness of the restoring springs does not necessarily reduce bearing displacements, but it certainly results in increased isolation level forces and pier drifts; (2) semiactive controlled SAIVS device – switching based on the control algorithm developed which produces softening/negative tangential stiffness – reduces bearing displacements further than passive open and passive closed cases, while significantly reducing isolation level forces when compared to the passive closed case; (3) semiactive controlled case also maintains the pier drifts and deck acceleration either less than or within bounds of the passive open and closed cases; (4) the developed analytical model, which incorporates the nonlinear characteristics of sliding bearings and SAIVS device, captures the response of the bridge model satisfactorily and can be used to perform an extensive analytical study. Thus through analytical simulations and experimental tests, it is demonstrated that by incorporating the new SAIVS device into the sliding isolation system, the performance of sliding base-isolated bridges can be improved.

ACKNOWLEDGMENTS

Funding for this project provided by the National Science Foundation, NSF-CAREER Grant CMS – 9996290, is gratefully acknowledged.

REFERENCES

Agrawal, A.K., Yang, J.N. and He, W.L. 2003. ''Applications of Some Semiactive Control Systems to Benchmark Cable-stayed Bridge,'' *Journal of Structural Engineering*, 129(7): 884–894.

Carlson, J.D. and Chrzan, M.J. 1994. ''Magnetorheological Fluid Dampers,'' US Patent #5,277,281.

Gavin, H.P. 2001. ''Control of Seismically Excited Vibration using Electrorheological Materials and Lyapunov Methods,'' *IEEE Transactions on Automatic Control*, 9(1):27–36.

Jabbari, F. and Bobrow, J. 2002. ''Vibration Suppression with Resettable Device,'' *Journal of Engineering Mechanics*, 128(9):916–924.

Jung, H., Park, K.S., Spencer, B.F. and Lee, I. 2004. ''Hybrid Seismic Protection of Cable-stayed Bridges,'' *Earthquake Engineering and Structural Dynamics*, 33(7):795–820.

Kawashima, K. and Unjoh, S. 1994. ''Seismic Response Control of Bridges by Variable Dampers,'' *Journal of Structural Engineering*, 120(9):2583–2601.

Kelly, J.M. 1997. *Earthquake-resistant Design with Rubber*, 2nd edn, Springer, NY

Kobori, T., Takahashi, M., Nasu, T., Niwa, N. and Ogasawara, K. 1993. ''Seismic Response Controlled Structure with Active Variable Stiffness System,'' *International Journal on Earthquake Engineering and Structural Dynamics*, 22(9):925–941.

Makris, N. 1997. ''Rigidity–plasticity–viscosity: Can Electro-rheological Dampers Protect Base Isolated Structures from Near Source Ground Motions?,'' *Earthquake Engineering and Structural Dynamics*, 26(5):571–591.

Makris, N. and Zhang, J. 2004. ''Seismic Response Analysis of a Highway Overcrossing Equipped with Elastomeric Bearings and Fluid Dampers,'' *Journal of Structural Engineering*, 130(6):830–845.

Mills, R.S., Krawinkler, H. and Gere, J.M. 1979. ''Model Tests on Earthquake Simulators Development and Implementation of Experimental Procedures,'' Report No. 39, John A. Blume Earthquake Engineering Center, Stanford University, USA.

Nagarajaiah, S. 1994. ''Fuzzy Controller for Structures with Hybrid Isolation System,'' *Proceedings of the 2nd World Conference on Structural Control*, Wiley, N.Y., TA2: 67–76.

Nagarajaiah S. and Mate, D. 1998. ''Semi-active Control of Continuously Variable Stiffness System,'' In: *Proceedings of the Second World Conference on Structural Control*, Kyoto, Japan, July 1, pp. 397–406.

Nagarajaiah, S., Reinhorn, A.M. and Constantinou, M.C. 1991a. ''3D-BASIS: Nonlinear Dynamic Analysis of Three-dimensional Base Isolated Structures - Part II,'' Report No. NCEER-91-0005, National Center for Earthquake Engineering Research, SUNY, Buffalo, NY.

Nagarajaiah, S., Reinhorn, A.M. and Constantinou, M.C. 1991b. ''Nonlinear Dynamic Analysis of 3D-Base Isolated Structures,'' *Journal of Structural Engineering*, 117(7):2035–2054.

Nagarajaiah, S., Riley, M.A. and Reinhorn, A.M. 1993. ''Control of Sliding Isolated Bridge with Absolute Acceleration Feedback,'' *Journal of Engineering Mechanics*, 119(11):2317–2332.

Narasimhan, S. and Nagarajaiah, S. 2005. ''A STFT Semiactive Controller for Base Isolated Buildings with Variable Stiffness Isolation Systems,'' *Engineering Structures*, 27(4):514–523.

Nasu, T., Kobori, T., Takahashi, M., Niwa, N. and Ogasawara, K. 2001. ''Active Variable Stiffness System with Non-resonant Control,'' *Earthquake Engineering Structural Dynamics*, 30(11): 1597–1614.

Sahasrabudhe, S. 2002. ''Semi-active Control of Sliding Isolated Buildings and Bridges with Variable Stiffness and Damping Systems,'' PhD Thesis, Rice University, Houston, Texas, USA.

Sahasrabudhe, S. and Nagarajaiah, S. 2005a. ''Experimental Study of Sliding Base-isolated Buildings with Magnetorheological Dampers in Near-fault Earthquakes,'' *Journal of Structural Engineering* (*ASCE*), 131(7), in press.

Sahasrabudhe, S. and Nagarajaiah, S. 2005b. "Semiactive Control of Sliding Isolated Bridges using MR Dampers: An Experimental and Numerical Study," *Earthquake Engineering and Structural Dynamics* (published online on January 31, 2005).

Shen, T.J., Tsai, M., Chang, K. and Lee, G. 2004. "Performance of a Seismically Isolated Bridge under Near-fault Earthquake Ground Motions," *Journal of Structural Engineering*, 130(6): 861–868.

Spencer, B.F. and Nagarajaiah, S. 2003. "State of the Art Structural Control," *Journal of Structural Engineering*, 129(7):845–856.

Spencer, B.F., Dyke, S.J., Sain, M.K. and Carlson, J.D. 1997. "Phenomenological Model of a Magnetorheological Damper," *Journal of Engineering Mechanics*, 123(3):230–238.

Symans, M.D. and Kelly, S.W. 1999. "Fuzzy Logic Control of Bridge Structures using Intelligent Semiactive Seismic Isolation System," *Earthquake Engineering Structural Dynamics*, 28:37–60.

Tsopelas, P., Okamoto, S., Constantinou, M.C., Ozaki, D. and Fujii, S. 1994. "Experimental and Analytical Study of Systems consisting of Sliding Bearings, Rubber Restoring Devices and Fluid Dampers," Report No. NCEER-94-0002, Vol. I, National Center for Earthquake Engineering Research, State University of New York, Buffalo, NY.

Wen, Y.K. 1976. "Method of Random Vibration of Hysteretic Systems," *Journal of Engineering Mechanics*, 102(2):249–263.

Yang, J.N., Wu, J.C., Kawashima, K. and Unjoh, S. 1995. "Hybrid Control of Seismic-exited Bridge Structures," *Earthquake Engineering and Structural Dynamics*, 24(11): 1437–1451.

Yang, J.N., Kim, J.H. and Agrawal, A. 2000 "Resetting Semiactive Stiffness Damper for Seismic Response Control," *Journal of Structural Engineering*, 126(12):1427–1433.